Title

NEUTRON AND PHOTON EMISSION FROM DYSPROSIUM AND TERBIUM COMPOUND NUCLEI: RANGE DISTRIBUTIONS

Authors

Alexander, John M.
Gilat, Jacob
Sisson, David H.

Publication Date

1964-03-10

University of California

Ernest O. Lawrence Radiation Laboratory

NEUTRON AND PHOTON EMISSION FROM DYSPROSIUM AND TERBIUM COMPOUND NUCLEI: RANGE DISTRIBUTIONS

John M. Alexander, Jacob Gilat, and David H. Sisson

March 10, 1964

Berkeley, California

DISCLAIMER

Submitted for publication in
Phys. Rev.

UCRL-11187

UNIVERSITY OF CALIFORNIA

Lawrence Radiation Laboratory
Berkeley, California

AEC Contract No. W-7405-eng-48

NEUTRON AND PHOTON EMISSION FROM DYSPROSIUM AND TERBIUM COMPOUND NUCLEI: RANGE DISTRIBUTIONS

John M. Alexander, Jacob Gilat, and David H. Sisson

March 10, 1964

NEUTRON AND PHOTON EMISSION FROM DYSPROSIUM AND TERBIUM COMPOUND NUCLEI: RANGE DISTRIBUTIONS*

John M. Alexander,† Jacob Gilat,‡ and David H. Sisson

Lawrence Radiation Laboratory
University of California
Berkeley, California

March 10, 1964

ABSTRACT

Electrostatic collection of Tb and Dy recoils stopped in H_2 gas has been explored, and found satisfactory for the study of recoil range distributions. For the reactions $Pr^{141}(C^{12},4n)Tb^{149g}$, $Nd^{146}(B^{11},8n)Tb^{149g}$, $Nd^{144}(C^{12},xn)Dy^{156-x}$, and $Ce^{140}(O^{16},xn)Dy^{156-x}$ (where x = 5, 6, or 7), the range distributions are determined by the initial velocity distributions of the recoiling reaction products. Comparison of range and angular distributions indicates nearly isotropic neutron emission for the latter two reactions. A similar comparison indicates a strong forward-backward peaking of the neutrons in the former two reactions. Values of the average total neutron and photon energies emitted in these reactions are derived from the results.

I. INTRODUCTION

This paper is one of a series that explores the properties of compound nuclei of energy up to 120 MeV and angular momentum up to 100 $\hbar$. In previous studies measurements were made of the formation cross sections, recoil ranges, and angular distributions of Dy and Tb nuclides produced in heavy-ion-induced reactions. The average range values give strong evidence for neutron emission symmetric about 90 deg in the c.m. system.[1] Also, the excitation functions exhibit a clear regularity and depend on the average angular momenta of the compound systems.[2] These observations are interpreted as evidence for the applicability of the compound nucleus and statistical models to these reactions.

The average total energies of the emitted neutrons and photons were obtained from an analysis of the angular distributions of these Dy and Tb products.[3] In this analysis, isotropic neutron emission was assumed. It was pointed out that the assumption of isotropy could be tested by measuring the range straggling of the products due to their distribution of velocities. The range straggling in aluminum foils was found to result primarily from the stopping process and from inhomogeneities of the foils.[1]

This report deals with the electrostatic collection of Dy and Tb recoils stopped in hydrogen gas and discusses the use of this technique to determine range distributions. Theoretical considerations and various tests of the collection method indicate that the range distributions thus obtained are primarily due to the velocity distributions of the products. The comparison of these range distributions with the angular distributions verifies the approximation of isotropic neutron emission for the reactions $Nd^{144}(C^{12}, 5n)Dy^{151}$; $Nd^{144}(C^{12},6n)Dy^{150}$; $Nd^{144}(C^{12},7n)Dy^{149}$; $Ce^{140}(O^{16},5n)Dy^{151}$;

$Ce^{140}(O^{16},6n)Dy^{150}$; and $Ce^{140}(O^{16},7n)Dy^{149}$; for these reactions the previously reported[3] values of average total neutron and photon energies (T_n and T_γ) are confirmed. A rather pronounced forward-backward peaking is indicated for neutron emission in the reactions $Nd^{146}(B^{11},8n)Tb^{149g}$ and $Pr^{141}(C^{12},4n)Tb^{149g}$, and corrected values for the neutron and photon energies (T_n and T_γ) and the angular distributions of the neutrons are derived from the data by an approximate method.

II. EXPERIMENTAL METHOD

A. Apparatus and Typical Experimental Conditions

We have studied Dy and Tb recoils from reactions of heavy ions (B^{11}, C^{12}, O^{16}, and Ne^{20}) with various targets, made of thin layers of the appropriate separated isotopes, evaporated onto Al backing 0.00025 in. thick. The recoils are initially directed in a narrow cone along the beam direction (< 15 deg).[3] They are slowed down in H_2 gas, collected on two parallel plates covered with Al foil, and maintained at a potential difference from 500 to 2000 v. The spatial distribution of the radioactive products is determined by cutting the collector foil into strips, which are assayed for α activity as previously described.[1,2,3] A schematic diagram of the apparatus is shown in Fig. 1. The beam enters the gas-tight chamber through a 0.001-in. dural window, and passes through two 3/8-in. collimators, spaced about 3 in. apart. The second collimator also serves as target mount. Energy-degrading aluminum foils, when used, are mounted on the first collimator. After passing through the target, the beam is monitored by a Faraday cup, separated from the chamber by a second window. This gas-stopping technique has been used previously by several other workers.[4,5,6]

The chamber and U-tube mercury manometer were flushed several times with hydrogen gas before each exposure. The chamber was then filled to the desired pressure and sealed. Opposite potentials, usually 1000 v with respect to the grounded target mount and chamber walls, were applied to the collector plates. Pressure readings were taken before and after each exposure; the final pressure was never more than 0.05 in. greater than the initial pressure and a difference of 0.02 in. was typical.

Most of the recoil collection (40 to 70%) was on the negative plate. The positive plate collected about one-tenth as much as the negative. The lack of reproducibility of the collection efficiency is attributed to variable levels of impurities in the gas. There was no detectable dependence of collection efficiency on voltage, but it seemed to be lowered by increasing gas pressure.

The Hilac furnishes 3-msec beam pulses at a frequency of 10 to 15 pulses/sec. Exposure to average beam current greater than 75 mμA gave rise to an upward drifting of the collected recoils. The drift distance increased with increasing beam intensity and is presumed to be due to convection currents. If the ions move toward the plates with a mean velocity of $\approx 10^4$ cm/sec (as discussed in Sec. II.B) then convection currents of $\approx 10^3$ cm/sec or $\approx$ 20 mph would cause detectable upward drifts. The width of the range distributions in the beam direction was not appreciably affected by even the largest upward drift observed ($\approx$ 1/4 inch). Experiments were performed at low beam intensities ($\approx$ 50 mμA) to minimize any possible convection effects, as well as to avoid discharges in the chamber.

Under these conditions the plate voltage was not affected by the beam, and the ion current in the chamber was proportional to the beam intensity. The profile of the pulses of ion current in the chamber was

essentially the same as those of the beam. Under typical experimental conditions there were about 3×10^9 projectiles per beam pulse, or (assuming 30 eV per ion pair) about 5×10^{14} ion pairs produced. This corresponds to an ion density in the direct beam of about 3×10^{13} ions/ml, compared to about 10^{19} molecules per-ml of gas. We actually collected about (2 to 10)$\times 10^{12}$ positive ions (measured by the integrated current on the negative plate), and 3 to 10 times as many negative ions per beam burst. Presumably, the difference between positive and negative ion collection is due to electrons ejected from the target and window foils, Extensive recombination of the ionized gas molecules must take place, but 40 to 70% of the rare earth recoils are collected on the negative plate.

B. Tests of the Method

One cannot be sure a priori of the relationship between the recoil range and the point at which a recoil is collected, and the horizontal distance from target to point of collection may differ from the projected recoil range. Therefore a variety of tests have been performed. The results of typical experiments are shown in Figs. 2 and 3. A Gaussian function (indicated by the straight lines on the probability plot) provides a good fit to most of the observed distribution. In most experiments a "short-range tail" is observed, which is not fit by the Gaussian plots. (This tail never contains more than 3% of the recoils collected; however, the magnitude and shape are not reproducible.)

If this tail is neglected, the range distributions can be represented by the median range R_0 and standard deviation σ (or range straggling parameter, $\rho = \frac{\sigma}{R_0}$) as determined from the Gaussian fit. Alternatively, the average range is given by

$$\langle R \rangle = \sum_i F_i d_i \ , \qquad (1)$$

where F_i is the fraction of the collected activity on the ith strip, and d_i is the projected distance from the target to the center of this strip (increased by the stopping equivalent in H_2 of one-half the target thickness); the mean range fluctuation is given by

$$\langle \Delta R^2 \rangle / \langle R \rangle^2 = \sum_i F_i (d_i - \langle R \rangle)^2 / \langle R \rangle^2 . \qquad (2)$$

As shown in Tables I and II, the difference between R_0 and $\langle R \rangle$ is negligible, and these two parameters are practically interchangeable. The difference between ρ^2 and $\langle \Delta R^2 \rangle / \langle R \rangle^2$ depends on the magnitude of the short-range tail. This tail was essentially eliminated by a wide-angle collimator, which removed recoils at very large angles (position c in Fig. 1), as shown in Fig. 4. The collimator accepted all angles with appreciable cross sections as determined by angular-distribution measurements.[3] These facts and the inability to reproduce the shape of the tail lead us to believe that the tail is mainly of instrumental origin. Therefore we eliminate the tail from our analysis and use the Gaussian parameters R_0 and ρ. Standard deviations for a single determination of R_0 and ρ are about 2% and 5%, respectively.

The observed distributions of radioactivity may be affected by the following experimental factors: (a) scattering due to finite target thickness, (b) diffusion of recoil ions or atoms before collection, (c) drift due to convection currents, and (d) inhomogeneity of the electric field and its distortion by edge effects (primarily near the target itself). The field shape for a very similar arrangement has been discussed in some detail by

Bryde, Lassen, and Poulsen.[6] The target mount is the only source of bending of the field lines in the forward or backward directions, and this effect is shown to be negligible for average ranges of ≈ 3 to 6 inches.

The magnitude of diffusion and convection effects is related to the diffusion coefficient (D) for Dy in H_2 and the average collection time t; D varies inversely with pressure and can be estimated to be approximately 1 cm^2/sec at 1/2 atm.[7] The drift velocity of the ions is given by

$$\bar{v} = D E q/kT, \tag{3}$$

where E is the field strength, q the ionic charge, k Boltzmann's constant, and T the absolute temperature. The mean-square displacement due to diffusion is given by

$$\langle X^2 \rangle = Dt. \tag{4}$$

From these expressions we can conclude that if the recoil ions retain their positive charge until collection, the collection time t is about 10^{-4} sec and the diffusion distance is about 10^{-2} cm. This would have essentially no effect on the initial range distribution. Significant diffusion could occur only if the recoils in the gas were neutralized for a time greater than ≈ 1/4 sec. We have not measured the collection time directly, but we estimated its effect on the recoil distributions by varying field strength, gas pressure, and interplate distance. The variance σ^2 of the observed distribution is related to the collection time by the equations

$$\sigma^2 = \sigma_r^2 + \sigma_d^2 \quad \text{and} \quad \sigma_d^2 = 2 Dt, \tag{5}$$

in which σ_r^2 and σ_d^2 denote respectively the contributions of the range distribution and of diffusion to the observed variance. Table I shows the result of several illustrative experiments. The first four columns give the experiment number, beam energy, gas pressure, and potential difference and distance between the plates; the last columns give the experimental results. Comparison of experiments 1 and 2 indicates that the Gaussian parameters R_0 and ρ do not depend on target thickness. Also, it is clear from the same experiments that the short-range tail can be only partially attributed to scattering in the target layer.

Comparison of experiments 3 and 4 shows that the values of R_0 and ρ (for ranges of ≈ 4 in.) are independent of the field strength. Similarly, experiments 4 and 5 indicate insensitivity to distance between the plates for comparable field strengths. And, most revealing of all, experiments 5 and 6 show that R_0 and ρ are insensitive to pressure. These experiments vary the time required to collect an ion (average path length divided by average velocity) by a factor of approximately 9/4. If diffusion played a leading role in determining the measured distribution, then the standard deviation σ ($\sigma = R_0 \rho$) would increase with increasing collection time [see Eq. (5)]. This is certainly not the case. We conclude that for average ranges of ≈ 4 to 6 inches the standard deviation from diffusion is negligible (< 0.1 in.).

Ranges of about 2 in. do exhibit an instrumental broadening, as shown by experiments 7 and 8. Although the standard deviation observed in experiment 7 is only 0.25 in., the ρ value is $\approx 25\%$ greater than that found in experiments 3 to 6. We attribute the additional broadening (≈ 0.05 in.) to distortion of the electric field in the region near the target mount. The comparison of experiments 7 and 8 shows that the distribution (for $R_0 \approx 2$ in.) is broadened by an increased distance between the plates. Even

though an instrumental broadening was observed in experiment 7, the small standard deviation of about 1/4 in. provides additional evidence that diffusion broadening is negligible if the average range is about 4 in. ($\sigma \approx 0.4$ in. in this case, and a 20% diffusion effect would result in a standard deviation due to diffusion $\sigma_d \approx 0.24$ in., which is incompatible with experiment 7).

The picture of the collection process that emerges from these experiments is as follows. A recoiling ion is ejected from the thin target layer and brought to an epithermal energy in about 10^{-7} sec. Most (40 to 70%) of the ions either retain their positive charge for the 10^{-4} second required for collection or are reionized positively by the ionizing radiation during the beam pulse of ≈ 3 msec. The collection of neutral atoms is negligible as shown by inefficient collection on the positive plate. Diffusion of the recoils leads to a root-mean-square horizontal displacement of less than 0.1 in. This sets an upper limit of ≈ 0.06 sec, or about 2 beam bursts for collection. The width of the range distribution, as characterized by ρ, is determined by the initial distribution of recoil velocities and by the statistical nature of the stopping process. It is not affected by target thickness or by instrumental sources.

III. RESULTS AND DISCUSSION

The results of the Tb and Dy stopping experiments are summarized in Table II. The initial energy of the Hilac beam was assumed to be 10.38 MeV/amu, and the range-energy curves of Northcliffe were used to calculate the energy losses in the window, degraders, and target backing.[8] A mass stopping-power ratio of 3.3 (mg H_2: mg Al) was assumed for estimating the energy loss in the gas between the window and the target. The error introduced by this assumption is negligible. The average recoil energies E_R were calculated from the bombarding energy E_b and from the mass numbers A of the bombarding, target, and recoil atoms designated, respectively, by the subscripts b, T, and R.

$$E_R = E_b A_b A_R/(A_b + A_T)^2 ; \qquad (6)$$

total momentum transfer was assumed.[3]

The range distributions are characterized by the Gaussian parameters R_0 (in units of length and mass per unit area) and ρ. The median range and the average range [Eq. (1)] never differ by more than a few percent (column 6). The difference between ρ and the mean range fluctuation [Eq. (2)] is more significant (column 7). This difference is clearly correlated with the magnitude of the short-range tail discussed above, as shown in columns 8 through 10, which give the ratios of the cumulative fractional activities F at $R_0 - \sigma$, $R_0 - 2\sigma$, and $R_0 + 2\sigma$ to the corresponding quantities F_G obtained from the Gaussian fits. As stated above, most of this tail is due to instrumental effects; therefore, we use the Gaussian parameters for our analysis. This procedure is supported by Monte Carlo calculations of the range distribution caused by the initial velocity spread of the recoiling ions,

according to which the distribution can be very closely approximated by a Gaussian function.[9]

A range-energy plot of the results of Table II is given in reference 10. For analyzing the data in terms of the initial velocity distribution of the recoiling atoms, it is convenient to represent the range-energy relationship by the empirical form

$$R_0 = kV_L^N , \tag{7}$$

in which V_L denotes the average recoil velocity in laboratory-system coordinates, and k and N are constants. In practice, it is found that the exponent N varies slowly with energy, i.e., Eq. (7) gives an adequate representation of restricted regions of the range-energy curve. Values of N as a function of the mean recoil energy were obtained by a least-squares fit of the data to a second-degree polynomial $R_0 = a E_R^2 + b E_R + c$, followed by logarithmic differentiation of this polynomial. The experiments with an O^{16} beam resulted in ranges systematically higher by a few percent than those obtained with C^{12} or Ne^{20} beams. In order to minimize errors due to such systematic differences, overlapping regions of the curve were fitted separately, and the values of N thus obtained were averaged. The results are summarized in Table III. In the middle portion of the curve (E_R of 6 to 15 MeV) the values are quite accurate, the probable error being ± 5%. Towards both ends of the curve the uncertainties increase to about ± 10%.

As pointed out earlier, both the recoil-velocity distribution and the stopping process are expected to contribute to the measured range straggling, i.e.,

$$\rho^2 = \rho_n^2 + \rho_s^2 , \tag{8}$$

where the subscripts n and s denote, respectively, the contributions of the nuclear and stopping processes. In reference 10, we make a detailed comparison of theoretical predictions with stopping measurements of Dy recoils in a series of gases from He to Xe. In general, the range straggling is in agreement with theoretical predictions, provided the single parameter of the theory is adjusted in accordance with the range-energy data. This result for heavier gases justifies the use of theoretical values of ρ_s^2 in H_2 to correct for the stopping effect. This correction is actually quite small, as the calculated values of ρ_s^2 are only about 10% of the observed values of ρ^2.

For isotropic neutron emission, the range straggling parameter ρ_n is related to the average total c.m. energy T_n of the emitted neutrons by the equation

$$T_n = \frac{3E_b A_b (A_b + A_T + A_R)^2 \rho_n^2}{4N^2 (A_b + A_T)^2} \qquad (9)$$

A similar relation connects the mean-square recoil angle $\langle \theta_L^2 \rangle$ (in the laboratory system) to T_n:

$$T_n = \frac{3E_b A_b (A_b + A_T + A_R)^2 \langle \theta_L^2 \rangle}{8(A_b + A_T)^2} \quad . \qquad (10)$$

If the neutron emission is not isotropic, these relations are no longer valid. For a given total neutron energy T_n, preferential emission in the forward-backward direction gives rise to a broadened velocity distribution along the beam, i.e., enhanced range straggling. At the same time, the recoil-velocity distribution perpendicular to the beam is narrowed, and the value of $\langle \theta_L^2 \rangle$ is reduced. The opposite effect would be observed if the neutron emission were peaked at 90 deg.

Thus, the parameter α, defined as

$$\alpha = \frac{2\rho_n^2}{N^2\langle\theta_L^2\rangle} \tag{11}$$

is a measure of the anisotropy of the neutron emission ($\alpha = 1$ for isotropic, $\alpha > 1$ for forward-backward peaking, and $\alpha < 1$ for 90 deg peaking). The exact calculation of T_n for $\alpha \neq 1$ is difficult, since in this case both the recoil probability W and recoil velocity V are functions of the c.m. angle θ.

If we ignore the dependence of V on θ, and represent the angular distribution in the c.m. system by

$$W(\theta) = a + b\cos^2\theta \ , \tag{12}$$

we obtain the following approximate relationships for the average total neutron energy:

$$\begin{aligned} T_n &= \frac{3E_bA_b(A_b + A_T + A_R)^2\langle\theta_L^2\rangle}{8(A_b + A_T)^2} \cdot \frac{2+\alpha}{3} \\ &= \frac{3E_bA_b(A_b + A_T + A_R)^2\rho_n^2}{4N^2(A_b + A_T)^2} \cdot \frac{2+\alpha}{3\alpha} \ , \end{aligned} \tag{13}$$

and for the anisotropy, we obtain

$$\frac{d\sigma(0^\circ) - d\sigma(90^\circ)}{d\sigma(90^\circ)} = \frac{b}{a} = \frac{5(\alpha - 1)}{3 - \alpha} \ . \tag{14}$$

The average total photon energy is given by

$$T_\gamma = E_a - T_n \tag{15}$$

where $E_a = E_{c.m.} + Q$ is the total available excitation energy. The measured values of α have uncertainties of $\approx 15\%$, which correspond to errors of 60% or more in the anisotropy parameter b/a, as determined by Eq. (14). Therefore, anisotropies deduced from measurements of ρ and $\langle\theta_L^2\rangle^{1/2}$ can be used only qualitatively. Nevertheless, the total neutron energy T_n as given by Eq. (13) is quite insensitive to uncertainties in the value of α, and the error introduced by a 15% uncertainty will be 5 to 9%. The final values of T_n are, therefore, uncertain by $\approx \pm 15\%$ and the relative values by about $\pm$ 10%. Table IV shows the values of ρ_n^2 and α for the reactions studied. Values of N were taken from Table III, and values of $\langle\theta_L^2\rangle$ were interpolated from reference 3. For experiments with a Ne^{20} beam, the values of $\langle\theta_L^2\rangle$ were estimated from Eq. (10) and Fig. 5 of reference 3, with the assumption that the general trends obtained with other reactions can be extrapolated to Ne^{20} beams and eight or nine evaporated neutrons.[11]

The anisotropy is determined by the correlation between the angular momentum $\underline{J}$ of the compound nucleus and the orbital angular momentum $\underline{\ell}$ of the evaporated neutrons. For a level density proportional to $\exp[-J^2/2\mathcal{I}T]$, Ericson and Strutinski have derived the following relationship for the anisotropy parameter:[12]

$$\frac{b}{a} = \frac{\hbar^4\langle J^2\rangle\langle \ell^2\rangle}{4\mathcal{I}^2T^2} \tag{16}$$

where $\mathcal{I}$ and T are, respectively, the moment of inertia and the nuclear temperature of the residual nucleus, and $\hbar$ is Planck's constant. At reasonably high excitation energies, the moment of inertia is expected to be essentially equal to that of a rigid body. For neutron emission from a rigid sphere of radius $1.2A^{1/3}$ fermis, Eq. (16) yields a value of ≈ 0.2 for b/a, if $\langle J^2 \rangle = 10^3$, $\langle \ell^2 \rangle = 10$, and $T = 2$ MeV.

It is quite likely that in neutron emission the removal of excitation energy is much more rapid than the removal of angular momentum.[13] Therefore Eq. (16) may not be valid for the last neutron (or possibly neutrons) emitted. Due to the scarcity of low-lying high-spin levels, the angular momentum of the last neutron is probably strongly aligned antiparallel to the angular momentum of the emitting nucleus, and the angular distribution of this neutron probably approaches the classical limit of $1/\sin\theta$. From these considerations, the gross angular distribution, averaged over all the neutrons in an evaporation chain, is expected to be approximated by $b/a < 1$, or $\alpha < 1.33$.

This prediction is verified by the values of α in Table IV for the reactions $Nd^{144}(C^{12},xn)Dy^{156-x}$ and $Ce^{140}(O^{16},xn)Dy^{156-x}$, with $x = 5,6$, or 7. These values of α are all less than 1.4 and no significant correction is required for the corresponding values of T_n and T_γ in reference 3. If we assume that only the last neutron is strongly anisotropic, then the average gross anisotropy should decrease with increasing number of evaporated neutrons. Although the differences between the different reactions border on experimental errors, the results seem to indicate such a decrease. For the $Ce^{140}(O^{16},7n)Dy^{149}$ reaction, the average value of α actually drops slightly below 1. This provides an a posteriori justification of the assumptions used to derive ρ_n from the measured ρ, since any further corrections would lead to neutron emission peaked at 90 deg, in marked contradiction with theory.

For the very similar reactions of Ne^{20} with Ba^{136} and Ba^{138}, the values of α appear to be significantly higher (1.2 to 1.7). However, as explained above, these values are not based on directly measured values of $\langle\theta_L^2\rangle$, and therefore are less certain than those obtained from C^{12} and O^{16} reactions. For the Ne^{20} reactions, N is derived from the upper portion of the range-energy curve; it is therefore subject to considerably larger errors. In addition, the relative importance of small diffusion effects increases with decreasing ρ, and the energy spread of the degraded beam (larger for the more highly ionizing Ne^{20} than for either O^{16} or C^{12}) may also begin to affect these quite narrow distributions. Thus, the apparent anisotropy could be due to systematic errors in the experimental values of ρ^2. In view of these uncertainties we have not calculated T_n from the Ne^{20} results.

A surprising result of this study is the large anisotropy indicated for the reactions $Pr^{141}(C^{12},4n)Tb^{149g}$ and $Nd^{146}(B^{11},8n)Tb^{149g}$. Reactions of this type, which lead to the low-spin member of an isomeric pair, are expected to proceed selectively from compound states of lower-than-average spin. Previously reported cross-section data imply that the particular reactions under study select compound states of $\langle J\rangle < 7.5$.[14] In order to account for the observed anisotropy, these reactions must select the rare neutron-evaporation chains in which all the orbital angular-momentum vectors are essentially antiparallel to that of the compound system. For this case of strong correlation, the angular distribution of the neutrons is given classically as $W(\theta) \propto 1/\sin\theta$, which corresponds to $\alpha = 2$, and the experimental values are very close to this value.

At first glance the large anisotropies implied by this work are difficult to reconcile with the argument for the compound systems of low spin presented in reference 14. However, it is certainly possible that the

production of Tb^{149g} proceeds through compound nuclei of lower-than-average spin, and still gives rise to much higher than-average neutron anisotropies. If a sizable fraction of the evaporation chains is accompanied by appreciable angular-momentum removal ($\Delta J > 2x$), large anisotropy would result. Such a situation could obtain even for a collection of compound nuclei with average spin of about 7.5, provided the collection contains a sufficient fraction of all compound nuclei to account for the observed cross section. (This would correspond to a rather long tail on curve B in Fig. 3 of reference 14.)

For $W(\theta) \propto 1/\sin\theta$, Eq. (13) becomes

$$T_n = \frac{E_b A_b (A_T + A_b + A_R)^2}{2(A_b + A_T)^2} \langle \theta_L^2 \rangle$$

$$= \frac{E_b A_b (A_T + A_b + A_R)^2 \rho_n^2}{2(A_b + A_T)^2 \, N^2} \qquad (17)$$

Although Eq. (17) is derived from a different angular distribution $W(\theta)$ than that used for Eq. (13), it yields the same neutron energy T_n as that obtained from Eq. (13) with $\alpha = 2$. Therefore, our measurements cannot distinguish between the forward-backward peaking associated with $W(\theta) = a + b\cos^2\theta$ with $b/a = 5.0$ (corresponding to $\alpha = 2$), and the very strong peaking associated with the $1/\sin\theta$ distribution.

Values of b/a, T_n and T_γ for the two reactions [obtained from Eqs. (13), (14) and (15)], together with their respective errors, are tabulated in Table V. Q values were obtained from Seeger's nuclear mass tables.[15] Table V constitutes a substantial correction to the previously reported

energetics of these reactions. Almost all the available excitation energy is taken up by the neutrons, and the total photon energies are very small. Normally, the photons play an important role in the de-excitation of the compound system, presumably in the removal of angular momentum. Since in this case an unusually large portion of the angular momentum is taken up by the neutrons, the nuclei can de-excite without appreciable γ emission.

IV. SUMMARY

This paper concludes a series of experimental studies of the energetics of neutron and photon emission in the reactions (C^{12} or O^{16}) + (Nd^{144} or Ce^{140}) $\rightarrow$ Dy^{156*} $\rightarrow$ 5, 6, or 7n + $Dy^{151,150,}$ or ^{149}, C^{12} + Pr^{141} $\rightarrow$ Tb^{153*} $\rightarrow$ Tb^{149g} + 4n, and B^{11} + Nd^{146} $\rightarrow$ Tb^{157*} $\rightarrow$ Tb^{149g} + 8n. Cross sections,[2,14] angular distributions,[3] average ranges,[1] and range dispersions have been measured. The average range measurements indicate that neutron emission is essentially symmetric about 90° in the c.m. system. Measurements of angular and range distributions lead to an unambiguous determination of the average total neutron and photon energies (T_n and T_γ). For reactions leading to the Dy^{156*} compound system, neutron emission is approximately isotropic and the average total photon energy is a rapidly increasing function of excitation energy. In the production of Tb^{149g} (low spin) from Tb compound systems, neutron emission is strongly peaked forward and backward, and very little energy is dissipated by photons.

These results provide a body of data for delimitation of nuclear-level density at high energy and angular momentum. However, a more refined calculation of nuclear evaporation than has been performed to date would be required for this purpose.

ACKNOWLEDGMENT

We would like to thank the Hilac operating crew for their help in the experiments.

FOOTNOTES AND REFERENCES

*Work performed under the auspices of U. S. Atomic Energy Commission.

†Present address: State University of New York, Stony Brook, Long Island, N. Y.

‡IAEA fellow from the Israel Atomic Energy Commission, Soreq Research Establishment, Yavneh, Israel.

1. John M. Alexander and David H. Sisson, Phys. Rev. 128, 2288 (1962).
2. John M. Alexander and Gabriel N. Simonoff, Phys. Rev. 133, B93 (1964).
3. Gabriel N. Simonoff and John M. Alexander, Phys. Rev. 133, B104 (1964).
4. Albert Ghiorso and Torbjorn Sikkeland, (Lawrence Radiation Laboratory) private communication.
5. Ernest W. Valyocsik, Range and Range Straggling of Heavy Recoil Atoms (Master's thesis) Lawrence Radiation Laboratory Report UCRL-8855, 1959 (unpublished).
6. Lise Bryde, N. O. Lassen and N. O. Roy Poulsen, Kgl. Danske Videnskab. Selskab, Mat. Fys. Medd. 33, No. 8 (1962).
7. Wilhelm Jost, Diffusion in Solids, Liquids, Gases (Academic Press, Inc., New York, 1952).
8. Lee C. Northcliffe, Phys. Rev. 120, 1744 (1960).
9. Lawrence L. Altman (Lawrence Radiation Laboratory), private communication.
10. Jacob Gilat and John M. Alexander, Stopping of Dysprosium Ions in Gases and Aluminum, Lawrence Radiation Laboratory Report UCRL-11055, January 1964 (unpublished)(submitted to Phys. Rev.).
11. Angular distributions of recoils from the $Ba^{136}(Ne^{20},7n)Dy^{149}$ and $Ba^{138}(Ne^{20},9n)Dy^{149}$ were consistent with this assumption; however, due to experimental difficulties, these measurements had to be carried out with fairly thick targets, and were not exactly comparable with those of reference 3. Therefore, we cannot consider the assumption to be verified.

12. Torleif Ericson and V. Strutinski, Nuclear Physics 8, 284 (1958).

13. Torleif Ericson, The Statistical Model and Nuclear Level Densities in Advances in Physics, N. F. Mott, Ed. (Taylor and Francis, Ltd., London, 1960) 9, 425.

14. John M. Alexander and Gabriel N. Simonoff, Phys. Rev. 130, 2383 (1963).

15. Philip A. Seeger, Nuclear Physics 25, 1 (1961).

Table I. Results of Some Experimental Tests.

Expt Number	E_b (MeV)	p (in. Hg)	Field[a] (volts/in.)	R_0 (in.)	R_0 (mg/cm^2)	ρ	$\frac{\langle R \rangle}{R_0}$	$\frac{\langle \Delta R^2 \rangle^{1/2}}{\langle R \rangle \rho}$
				$Nd^{144}(C^{12}, 7n)Dy^{149}$				
1[b]	113.0	8.05	2000/2	3.70	0.211	0.134	0.975	1.44
2[c]	113.0	8.07	2000/2	3.62	0.209	0.131	0.983	1.33
				$Ce^{140}(O^{16}, 7n)Dy^{149}$				
3[d]	145.0	11.83	2000/2	3.99	0.336	0.096	0.999	1.03
4[d]	145.0	11.76	1333/2	3.98	0.333	0.099	0.999	1.06
5[d]	145.0	11.70	2000/3	4.07	0.339	0.106	1.000	1.08
6[d]	145.9	7.78	2000/3	5.74	0.317	0.100	0.996	1.06
7[d]	142.7	22.38	666/1	2.04	0.324	0.123	0.995	1.15
8[d]	142.7	22.24	2000/3	2.01	0.317	0.178	0.950	1.54

[a] Potential difference divided by distance between plates

[b] Target thickness of 80 $\mu g/cm^2$

[c] Target thickness of 10 $\mu g/cm^2$

[d] Target thickness of 32 $\mu g/cm^2$

Table II. Stopping of Tb and Dy Ions in Hydrogen.

E_R[a] (MeV)	p (in. Hg)	R_0 (in.)	R_0 (mg/cm^2)	ρ	$\frac{\langle R \rangle}{R_0}$	$\frac{\langle \Delta R^2 \rangle^{1/2}}{\langle R \rangle \rho}$	$\frac{F(R_0 - \sigma)}{F_G}$	$\frac{F(R_0 - 2\sigma)}{F_G}$	$\frac{F(R_0 + 2\sigma)}{F_G}$
4.36[1]	3.90	4.22	0.117	0.144	0.973	1.47	1.16	3.41	1.00
4.90[1]	6.66	2.78	0.132	0.156	0.981	1.24	1.27	3.45	1.00
5.28[1]	4.65	4.08	0.135	0.152	0.988	1.25	1.10	2.23	1.00
5.55[2]	5.12	4.31	0.157	0.132	0.998	1.17	1.01	2.14	1.00
5.81[2]	6.60	3.28	0.153	0.141	0.980	1.37	1.29	3.67	1.00
5.82[2]	4.80	4.39	0.151	0.147	0.985	1.20	1.15	2.81	1.01
5.84[2]	4.81	4.56	0.156	0.144	0.995	1.08	1.11	1.50	0.99
5.98[3]	5.08	4.21	0.153	0.184	0.985	1.21	1.06	2.50	1.00
6.48[3]	6.24	4.13	0.167	0.191	0.984	1.20	1.08	2.42	1.00
6.96[4]	6.93	3.73	0.186	0.130	0.989	1.20	1.21	3.00	1.00
7.06[2]	6.93	3.69	0.183	0.144	0.989	1.20	1.21	3.00	1.00
7.08[3]	6.24	3.92	0.173	0.211	0.993	1.08	1.00	1.82	1.00
7.52[4]	7.83	3.57	0.192	0.126	0.962	1.45	1.25	3.35	1.00
7.57[5]	7.83	3.54	0.190	0.135	0.962	1.45	1.25	3.35	1.00
8.03[4]	6.09	4.74	0.206	0.137	0.995	1.15	1.00	1.31	1.00
8.04[4]	6.01	4.85	0.207	0.138	0.997	0.956	1.00	1.00	1.01
8.04[4]	6.00	4.88	0.208	0.142	1.01	0.965	1.00	1.27	1.01
8.04[4]	5.97	4.85	0.206	0.136	0.996	0.949	1.00	1.27	1.01
8.29[4]	8.50	3.56	0.212	0.131	0.981	1.35	1.20	3.14	1.00
8.29[4]	8.05	3.70	0.211	0.134	0.975	1.38	1.10	2.40	1.00
8.29[4]	8.07	3.62	0.209	0.131	0.983	1.33	1.03	2.27	1.00
8.35[5]	8.50	3.51	0.207	0.138	0.981	1.35	1.20	3.14	1.00
8.35[5]	8.05	3.65	0.209	0.146	0.975	1.38	1.10	2.40	1.00
8.58[6]	8.15	3.88	0.225	0.096	0.993	1.21	1.24	3.56	1.00
8.87[6]	7.54	4.30	0.230	0.106	0.992	1.19	1.09	2.14	1.00
10.01[6]	10.12	3.50	0.252	0.098	0.994	1.19	1.12	2.44	1.00
10.84[8]	10.27	3.55	0.259	0.094	0.987	1.47	1.24	3.40	1.00
10.91[7]	10.27	3.56	0.261	0.102	0.987	1.47	1.24	3.40	1.00
10.98[6]	10.27	3.58	0.261	0.100	0.987	1.47	1.24	3.40	1.00
11.75[8]	10.94	3.64	0.283	0.094	0.994	1.18	1.10	2.09	1.00
11.83[7]	10.94	3.64	0.283	0.098	0.994	1.18	1.10	2.09	1.00
13.04[8]	12.52	3.49	0.311	0.093	0.993	1.16	1.01	1.49	1.00
13.31[7]	12.52	3.50	0.312	0.098	0.993	1.16	1.01	1.49	1.00
14.16[8]	13.60	3.37	0.326	0.096	0.990	1.31	1.24	2.78	1.00
14.20[8]	11.83	3.99	0.336	0.096	0.999	1.03	1.00	1.21	1.00
14.20[8]	11.76	3.98	0.333	0.099	0.999	1.06	1.00	1.00	1.00
14.29[8]	7.78	5.74	0.317	0.100	0.996	1.06	1.00	1.57	1.00
14.40[9]	10.52	4.26	0.321	0.102	0.997	1.15	1.04	1.87	0.99
14.62[13]	11.42	3.87	0.322	0.099	0.995	1.24	1.14	2.59	0.99
14.72[12]	11.42	3.88	0.323	0.094	0.995	1.24	1.14	2.59	0.99
17.05[11]	12.00	4.21	0.359	0.095	0.994	1.30	1.04	2.16	1.00
17.27[9]	12.00	4.21	0.359	0.100	0.994	1.30	1.04	2.14	1.00
17.46[14]	12.64	4.05	0.365	0.091	0.994	1.14	1.10	2.38	1.00
17.58[13]	12.64	4.05	0.365	0.091	0.994	1.14	1.10	2.38	1.00
18.43[11]	13.44	3.98	0.381	0.090	0.999	1.15	1.03	2.00	0.99
18.56[10]	13.44	4.02	0.385	0.094	0.999	1.15	1.03	2.00	0.99
18.68[9]	13.44	4.01	0.384	0.092	0.999	1.15	1.03	2.00	0.99
20.70[11]	15.10	3.96	0.425	0.080	0.995	1.33	1.04	2.23	0.99
20.73[11]	14.97	3.93	0.418	0.084	0.999	1.18	1.00	1.54	0.99
20.87[10]	14.97	3.94	0.419	0.090	0.999	1.18	1.00	1.54	0.99
21.26[14]	15.63	3.74	0.414	0.092	0.998	1.15	1.00	1.50	1.00

a. The recoil energies were calculated by means of Eq. (6) for the following nuclear reactions:

1. $Pr^{141}(C^{12},4n)Tb^{149g}$
2. $Nd^{144}(C^{12},5n)Dy^{151}$
3. $Nd^{146}(B^{11},8n)Tb^{149g}$
4. $Nd^{144}(C^{12},7n)Dy^{149}$
5. $Nd^{144}(C^{12},6n)Dy^{150}$
6. $Ce^{140}(O^{16},5n)Dy^{151}$
7. $Ce^{140}(O^{16},6n)Dy^{150}$
8. $Ce^{140}(O^{16},7n)Dy^{149}$
9. $Ba^{138}(Ne^{20},7n)Dy^{151}$
10. $Ba^{138}(Ne^{20},8n)Dy^{150}$
11. $Ba^{138}(Ne^{20},9n)Dy^{149}$
12. $Ba^{136}(Ne^{20},5n)Dy^{151}$
13. $Ba^{136}(Ne^{20},6n)Dy^{150}$
14. $Ba^{136}(Ne^{20},7n)Dy^{149}$

Table III. Values of the Exponent N in $R_0 = kV_L^N$.

Average recoil energy, E_R(MeV)	N
6	1.80
9	1.71
12	1.61
15	1.50
18	1.38
21	1.26

Table IV. Comparison of Range Distributions with Angular Distributions.

E_b (MeV)	ρ_n^2	$\alpha = \frac{2\rho_n^2}{N^2\langle\theta_L^2\rangle}$
$Pr^{141}(C^{12},4n)Tb^{149g}$		
57.1	0.0188	$> 1.8_0$
64.1	0.0225	1.9_1
69.1	0.0214	1.6_8
$Nd^{146}(B^{11},8n)Tb^{149g}$		
89.9	0.0323	1.9_5
97.5	0.0350	1.6_9
106.5	0.0431	1.6_4
$Nd^{144}(C^{12},5n)Dy^{151}$		
74.5	0.0157	1.1_6
78.2[a]	0.0191[a]	1.3_9[a]
94.8	0.0193	1.3_5
$Nd^{144}(C^{12},6n)Dy^{150}$		
102.4	0.0169	1.1_2
113.0[b]	0.0189[b]	1.1_7[b]
$Nd^{144}(C^{12},7n)Dy^{149}$		
94.8	0.0155	1.1_3
102.4	0.0146	1.0_4
109.4[c]	0.0178[c]	1.1_9[c]
113.0[a]	0.0162[a]	1.0_3[a]

Table IV. (Cont.)

E_b (MeV)	ρ_n^2	$\alpha = \frac{2\rho_n^2}{N^2\langle\theta_L^2\rangle}$
$Ce^{140}(O^{16},5n)Dy^{151}$		
86.4	0.0080	1.0_6
89.3	0.0100	1.2_9
100.8	0.0085	1.0_9
110.6	0.0090	1.0_6
$Ce^{140}(O^{16},6n)Dy^{150}$		
110.6	0.0094	1.1_0
120.0	0.0087	0.9_5
133.1	0.0087	1.0_3
$Ce^{140}(O^{16},7n)Dy^{149}$		
110.6	0.0088	0.9_3
120.0	0.0079	0.9_0
133.1	0.0078	0.9_0
145.0[c]	0.0087[c]	1.0_2[c]
$Ba^{136}(Ne^{20},5n)Dy^{151}$		
118.6	0.0080	(1.5_3)[d]
$Ba^{136}(Ne^{20},6n)Dy^{150}$		
118.6	0.0090	(1.6_7)[d]
142.6	0.0076	(1.4_2)[d]
$Ba^{136}(Ne^{20},7n)Dy^{149}$		
142.6	0.0076	(1.4_1)[d]
173.6	0.0079	(1.4_8)[d]

Table IV. (Cont.)

E_b (MeV)	ρ_n^2	$\alpha = \frac{2\rho_n^2}{N^2\langle\theta_L^2\rangle}$
$Ba^{138}(Ne^{20},7n)Dy^{151}$		
119.0	0.0096	$(1.6_6)^d$
142.6	0.0093	$(1.6_4)^d$
154.4	0.0078	$(1.4_1)^d$
$Ba^{138}(Ne^{20},8n)Dy^{150}$		
154.4	0.0082	$(1.4_7)^d$
173.6	0.0075	$(1.4_1)^d$
$Ba^{138}(Ne^{20},9n)Dy^{149}$		
142.8	0.0084	$(1.4_4)^d$
154.4	0.0075	$(1.3_6)^d$
173.5[b]	0.0062[b]	$(1.2_0)^d$

a. Average of three experiments
b. Average of two experiments
c. Average of four experiments
d. Based on extrapolated values of $\langle\theta_L^2\rangle$.

Table V. Approximate Anisotropy and Average Energies for Reactions Leading to Tb^{149g}.

E_b (MeV)	$E_{c.m.} + Q$ (MeV)	$\frac{d\sigma(0^\circ)-d\sigma(90^\circ)}{d\sigma(90^\circ)}$	T_n (MeV)	T_γ (MeV)
$Pr^{141}(C^{12},4n)Tb^{149g}$				
57.1	5.6	> 3.3	7.7 ± 1.2	-2.1 ± 1.2
64.1	12.1	4.2	10.3 ± 1.5	1.8 ± 1.5
69.1	16.7	2.6	11.5 ± 1.7	5.2 ± 1.7
$Nd^{149}(B^{11},8n)Tb^{149g}$				
89.9	17.5	4.5	19.0 ± 2.9	-2.5 ± 2.9
97.5	24.6	2.6	24.3 ± 3.7	0.3 ± 3.7
106.5	32.9	2.4	34.0 ± 5.1	-1.1 ± 5.1

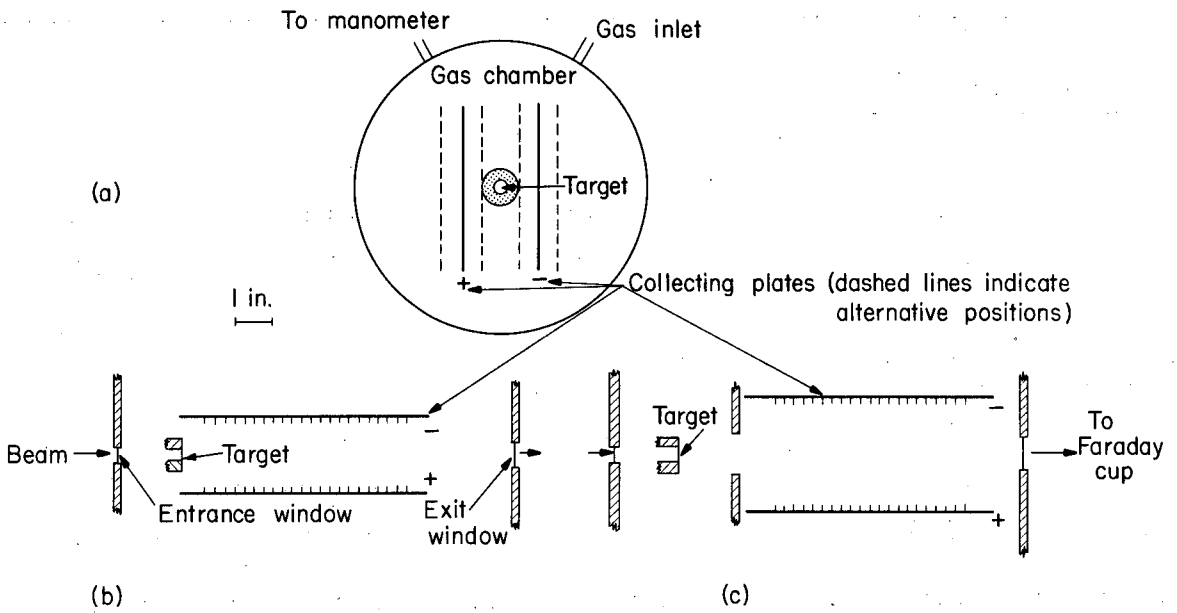

Fig. 1. Schematic diagram of recoil collection apparatus, showing the various collector positions: (a) front view; (b) top view, normal collector position; (c) top view, recessed collector position.

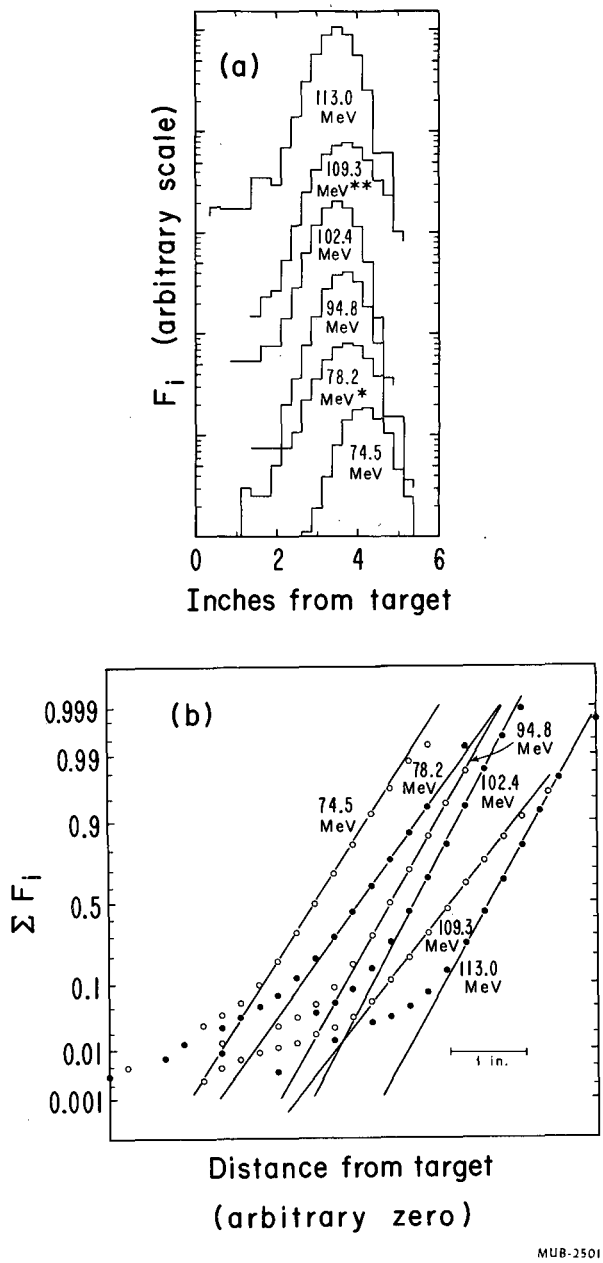

Fig. 2. (a) Range distribution histograms and (b) probability plots for the $Nd^{144}(C^{12},xn)Dy^{149-151}$ reactions. F_i denotes the fraction of total activity collected on the ith 1/4-in. strip. ΣF_i denotes the cumulative fraction of total activity collected through the ith strip. 0,0 - experimental points, solid lines - best Gaussian fit.

*0.5 inch further from target than indicated.

**1.0 inch further from target than indicated.

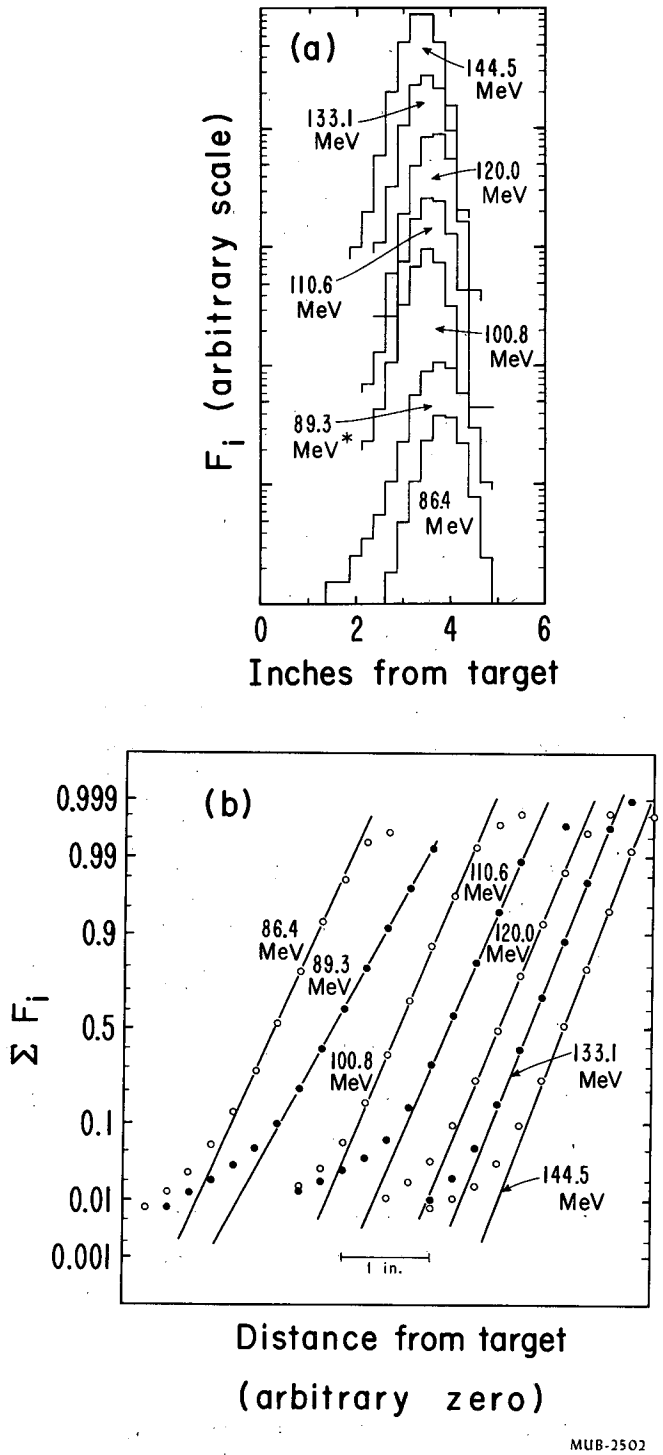

Fig. 3. (a) Range distribution histograms and (b) probability plots for the $Ce^{140}(O^{16},xn)Dy^{149-151}$ reactions. Notation as in Fig. 2.

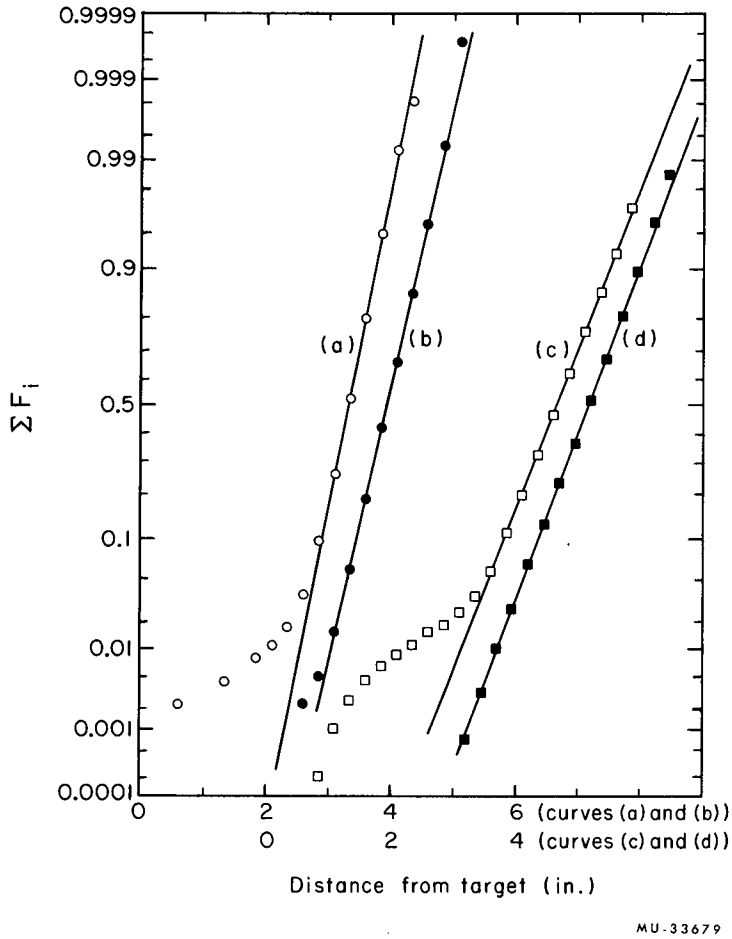

Fig. 4. Probability plots for the following range distributions:
(a) $Ce^{140}(O^{16},7n)Dy^{149}$; E_b = 144.5 MeV, p = 13.60 in. Hg, normal collector position
(b) $Ce^{140}(O^{16},7n)Dy^{149}$; E_b = 145.0 MeV, p = 11.83 in. Hg, recessed collector position
(c) $Nd^{144}(C^{12},7n)Dy^{149}$; E_b = 109.3 MeV, p = 6.09 in. Hg. normal collector position
(d) $Nd^{144}(C^{12},7n)Dy^{149}$; E_b = 109.4 MeV, p = 6.01 in. Hg, recessed collector position, plot (d) is displaced by 0.5 in. with respect to (c).